

# Neutron structure function via a maximum entropy analysis

Chengdong Han, Rong Wang,\* and Xurong Chen†

*Institute of Modern Physics, Chinese Academy of Sciences, Lanzhou 730000, China*

*State Key Laboratory of Heavy Ion Science and Technology,*

*Institute of Modern Physics, Chinese Academy of Sciences, Lanzhou 730000, China and*

*School of Nuclear Science and Technology, University of Chinese Academy of Sciences, Beijing 100049, China*

We employ the maximum entropy method to extract the valence quark distributions of the neutron at a low scale,  $Q_0^2$ . At this initial scale, the neutron is defined to contain only three valence quarks, with no contributions from sea quarks or gluons. The distributions of these initial valence quarks are constrained by principles from quark models, quark-hadron duality, and quark confinement. Employing the DGLAP equations supplemented by parton-parton recombination corrections, we derive the neutron structure function  $F_2^n$  at higher scales  $Q^2$ . The resulting ratio of the neutron to proton structure functions,  $F_2^n/F_2^p$ , aligns well with world data from deep inelastic scattering (DIS) on proton and deuteron targets, particularly when accounting for uncertainties from model-dependent corrections. Notably, this ratio is in agreement with the JLab MARATHON dataset, especially as  $x$  approaches 1. Additionally, our findings for  $F_2^n/F_2^p$  correspond well with the JLab BONuS experimental results after considering the impact of nucleon resonance contamination in the region  $x \gtrsim 0.4, 0.5, 0.6$ . We further compare our predictions for  $F_2^n/F_2^p$  and the  $u/d$  ratios in the limit as  $x \rightarrow 1$  with existing theoretical calculations. Finally, we observe a minor violation of isospin symmetry between the proton and neutron, evidenced by the differences in valence quark distributions and the first-order moments of these distributions.

## I. INTRODUCTION

The determination of the neutron structure function  $F_2^n$  [1–10] is essential for advancing our understanding of the quark structure within the nucleon. The relatively limited knowledge of neutron structure information, in contrast to that of the proton, is primarily due to the scarcity of neutron targets, making the study of  $F_2^n$  a topic of significant interest. Currently, most of the available neutron structure function information is extracted from a comprehensive review of global deep inelastic scattering (DIS) data obtained from proton, deuteron, tritium, and  $^3\text{He}$  targets throughout the full kinematic range. This extraction process also incorporates various nuclear correction models.

Recent advancements have emerged from the JLab MARATHON experiment [11], which utilized two high-resolution spectrometers for electron detection to measure the ratio of nucleon  $F_2$  structure functions, denoted as  $F_2^n/F_2^p$ , through deep inelastic electron scattering off  $^3\text{H}$  and  $^3\text{He}$  nuclei. A novel analytical technique exploiting the mirror symmetry of  $^3\text{H}$  and  $^3\text{He}$  significantly mitigated theoretical uncertainties associated with this extraction. The reported  $F_2^n/F_2^p$  ratio, spanning the Bjorken variable range  $0.19 < x < 0.83$ , constitutes a notable improvement relative to prior measurements conducted by SLAC and JLab. Additionally, the Barely Off-shell Nucleon Structure (BONuS) experiment at JLab [5, 7, 12] facilitated the measurement of quasi-free neutron structure function data across both nucleon-resonance and DIS regions by detecting low-momentum spectator protons at backward angles during semi-inclusive scattering with deuterons.

Over the past few decades, considerable interest has also been directed toward the ratio  $F_2^n/F_2^p$  at elevated values of the

Bjorken variable  $x$ . The neutron structure function  $F_2^n$  [13] and the corresponding  $F_2^n/F_2^p$  ratio are regarded as pivotal for determining the  $d/u$  (or  $u/d$  for the neutron) ratio in the limit as  $x$  approaches 1.

It is important to note that the analysis results of neutron structure functions obtained thus far do not stem from an authentic free neutron target. The challenges posed by the short lifetime of the neutron and the low energy and intensity of existing neutron beams have rendered direct experimental investigations of its internal structure impractical. Consequently, information regarding neutron structure is typically inferred from deuterium or  $^3\text{He}$  target data obtained via DIS measurements. The neutron structure function is subsequently deduced by applying corrections based on known proton structure functions, which necessitate model-dependent adjustments to account for nuclear binding, Fermi motion, EMC effects, final state interactions, and nucleon off-shell effects [14–18]. Despite these corrections, the extraction of the neutron structure function  $F_2^n$ , especially in the large  $x$  domain ( $x > 0.8$ ), remains fraught with uncertainties. Varied nuclear correction models yield divergent theoretical predictions for the  $F_2^n/F_2^p$  and  $d/u$  (or  $u/d$  for the neutron) ratios in the limit as  $x$  approaches 1 [3, 6, 19, 20].

In this work, we seek to determine the initial valence quark distributions at a scale  $Q_0^2$  for the neutron using the Maximum Entropy Method (MEM). This approach leverages existing structure information and properties of the neutron within the frameworks of quark models and quantum chromodynamics (QCD). The MEM has been effectively applied to investigate parton distributions of protons [21, 22], mesons [23, 24], and exotic hadrons such as the  $Z_c(3900)$  [25]. By employing DGLAP equations with nonlinear corrections [26–29] to evolve the nonperturbative neutron input obtained via MEM to higher scales, we will compare the resulting neutron structure function and  $F_2^n/F_2^p$  ratio with available experimental data. Furthermore, we will discuss our findings regarding the structure function ratio  $F_2^n/F_2^p$  and the  $u/d$  ratio for the

\* rwang@impcas.ac.cn

† xchen@impcas.ac.cn

neutron, contrasting them with predictions from various theoretical models in the limit as  $x$  approaches 1. Finally, we will compute the valence quark momentum distribution differences between protons and neutrons as functions of the Bjorken variable  $x$ , along with the first-order moments differences as functions of  $Q^2$ , to assess the extent to which protons and neutrons adhere to isospin symmetry.

## II. DETERMINING THE NONPERTURBATIVE INPUT BY MAXIMUM ENTROPY METHOD

Under certain constraints, the MEM principle can determine a reasonable initial valence quark distributions inside neutron, including constraints on the quark model, quark-hadron duality and quark confinement.

### A. Quark model constraints

The definition for Quark Model is a classification scheme that expounds the quantum numbers of the baryons and mesons by assuming that baryons are composed of three valence quarks and mesons are composed of a pair of quark and anti-quark. The parton distribution functions (PDFs) of nucleon at high  $Q^2$  obtained by performing DGLAP equations with parton-parton recombinations depend on the initial parton distributions at low scale  $Q_0^2$ . In this analysis, a naive non-perturbative input of the neutron only contains three valence quarks without other nonperturbative components (sea quarks and gluons), which is the simplest initial parton distribution input [26, 30–32]. In the view of dynamical PDF model, the sea quarks and gluons are radiatively generated from three valence quarks of neutron at high scale  $Q^2 > Q_0^2$ . We take the input scale  $Q_0^2 = 0.067 \text{ GeV}^2$  that is determined by the global QCD analysis of experimental data of proton [28]. The running strong coupling and parton-parton correlation length  $R$  which characterizes the strength parton-parton recombination corrections are determined by a large number of DIS experimental data at high  $Q^2$  [28, 33], which are the same as in the paper of valence quark distributions of the proton from MEM by Wang and Chen [21].

According to the framework of Quark Model, we have the valence sum rules and the momentum sum rule as constraints:

$$\int_0^1 u_v(x, Q_0^2) dx = 1, \int_0^1 d_v(x, Q_0^2) dx = 2. \quad (1)$$

$$\int_0^1 x[u_v(x, Q_0^2) + d_v(x, Q_0^2)] dx = 1. \quad (2)$$

### B. Quark-hadron duality

The most general function form to approximate valence quark distribution of nucleon is the time-honored canonical parametrization  $f(x) = Ax^B(1-x)^C$  [34]. The behav-

ior of elastic scattering is closely related to that of deep-inelastic electron-nucleon scattering, particularly about duality. Through finite-energy sum rules, Bloom and Gilman [35] derived the quantitative relations between the elastic scattering form factors and the deep-inelastic scattering and gave the ratio of the neutron structure function to the proton structure function under the assumption the ‘‘scaling’’ of the elastic form factors as  $x \rightarrow 1$  and  $q^2 \rightarrow \infty$ , as shown in Eq. 3.

$$F_2^n/F_2^p \sim (\mu_n/\mu_p)^2 = 0.47 = K, \quad (3)$$

where the  $\mu_n$  and  $\mu_p$  up are the magnetic moments of the neutron and proton, respectively. After considering the quark-hadron duality mentioned above, the parametrization of non-perturbative input for the neutron in this analysis is as follows,

$$\begin{aligned} u_v^n(x, Q_0^2) &= A_u x^{B_u} (1-x)^{C_u} [1 + D_u(1+x)^{C_u} \\ &\quad + E_u(1-x)^{2C_u}], \\ d_v^n(x, Q_0^2) &= (4K)A_d x^{B_d} (1-x)^{C_d} [1 + D_d(1+x)^{C_d} \\ &\quad + E_d(1-x)^{2C_d}]. \end{aligned} \quad (4)$$

From this parameterized Eq. 4 of the neutron valence quark, it can be seen that quark-hadron duality is automatically satisfied when  $x=1$ . Furthermore, considering the isospin symmetry of proton and neutron, the  $C_u = C_d^p=2.456$ ,  $C_d = C_u^p=1.000$ ,  $A_d = A_u^p=4.589$  here [21].

### C. Quark confinement

The quark confinement is a typical feature of strong interaction in Non-Abelian gauge field theory [36], which means all quarks are confined in a small region of hadron size. In this work, we use the Heisenberg uncertainty principle Eq. 5 as the constraint [21],

$$\sigma_X \sigma_P \geq \frac{\hbar}{2}, \quad (5)$$

where the  $\sigma_X$  is the standard deviation of the spacial distribution of one valence quark in the neutron, and the  $\sigma_P$  is the standard deviation of the valence quark momentum distribution in the neutron. Here,  $\sigma_X$  is directly related to the magnetic radius ( $R_m$ ) of the neutron, which is 0.864 fm [37]. A simple estimation of  $\sigma_X$  is  $\sigma_X = (2\pi R_m^3/3)/(\pi R_m^2) = 2R_m/3$ , for the neutron that is approximately spherical in shape. In addition,  $\sigma_X$  of each  $d$  valence quark is divided by  $2^{1/3}$  as there are two  $d$  valence quarks in the neutron. Then we get  $\sigma_{X_u} = 2R_m/3$  and  $\sigma_{X_d} = 2R_m/(3 \times 2^{1/3})$  for  $u$  and  $d$  valence quarks inside neutron respectively [21, 22]. Furthermore, the standard deviation of momentum fraction  $x$  at initial scale  $Q_0^2$  is defined as follows,

$$\sigma_x = \frac{\sigma_P}{M}, \quad (6)$$

where  $M$  is the rest mass of neutron [37]. Finally, the constraints for valence quark distributions from QCD color confinement and Heisenberg uncertainty principle [21] are written

as,

$$\begin{aligned} \sqrt{\langle x_u^2 \rangle - \langle x_u \rangle^2} &= \sigma_{x_u}, & \sqrt{\langle x_d^2 \rangle - \langle x_d \rangle^2} &= \sigma_{x_d} \\ \langle x_u \rangle &= \int_0^1 x u_v(x, Q_0^2) dx, & \langle x_d \rangle &= \int_0^1 x \frac{d_v(x, Q_0^2)}{2} dx \\ \langle x_u^2 \rangle &= \int_0^1 x^2 u_v(x, Q_0^2) dx, & \langle x_d^2 \rangle &= \int_0^1 x^2 \frac{d_v(x, Q_0^2)}{2} dx. \end{aligned} \quad (7)$$

#### D. Maximum entropy method

According to the constraints (Eqs. (1), (2), (3), (5) and (6)) already introduced above, there is only two unknown parameter  $B_u$  and  $B_d$  for Eq. 4. By applying MEM, one can determine the reasonable valence quark distributions under these constraints. The generalized information entropy of valence quark distributions for neutron is given by,

$$\begin{aligned} S = - \int_0^1 & \left[ u_v(x, Q_0^2) \text{Ln}(u_v(x, Q_0^2)) \right. \\ & \left. + 2 \frac{d_v(x, Q_0^2)}{2} \text{Ln} \left( \frac{d_v(x, Q_0^2)}{2} \right) \right] dx. \end{aligned} \quad (8)$$

The optimal parameterized initial valence quark distributions are given when the entropy  $S$  value is at the maximum. Fig. 1 shows the information entropy  $S$  of the valence quarks at the input scale  $Q_0^2$  as a function of the free parameter  $B_u$  and  $B_d$ . Entropy  $S$  value peaks at  $B_u = -0.0963$ ,  $B_d = 0.645$ . Hence the corresponding valence quark distributions from MEM are given by,

$$\begin{aligned} u_v(x, Q_0^2) &= 5.673 x^{-0.0963} (1-x)^{2.456} [1 - 0.631(1-x)^{2.456} \\ &\quad - 0.251(1-x)^{4.912}], \\ d_v(x, Q_0^2) &= 4.589 x^{0.645} (1-x)^{1.000} [1 - 2.774(1-x)^{1.000} \\ &\quad + 4.320(1-x)^{2.000}]. \end{aligned} \quad (9)$$

### III. RESULTS AND DISCUSSIONS

#### A. PDFs and structure functions of neutron

Parton distribution functions of neutron are evaluated dynamically starting from the obtained three valence quark input at the low scale  $Q_0^2$ . By performing DGLAP equations [38–40] with parton-parton recombination corrections [26–29], the parton distributions at an arbitrarily high scale  $Q^2$  can be determined with the nonperturbative input (Eq. 9). Fig. 2 shows the predicted momentum distributions of up and down valence quarks, sea quarks and gluon of neutron, at  $Q^2 = 1.5 \text{ GeV}^2$ .

The structure functions of nucleon reflect the characteristics of QCD defined by the asymptotic freedom of short distances and the confinement of quarks on the long distance scale. The unpolarized structure function  $F_2(x)$  is directly related to the

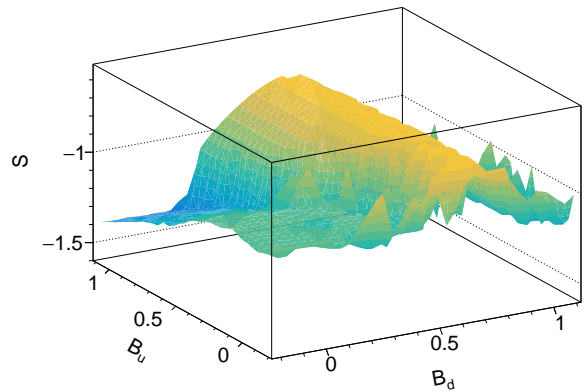


FIG. 1. Entropy  $S$  of valence quark distributions of neutron at  $Q_0^2 = 0.0671 \text{ GeV}^2$  is plotted as a function of the free parameter  $B_u$  and  $B_d$ .

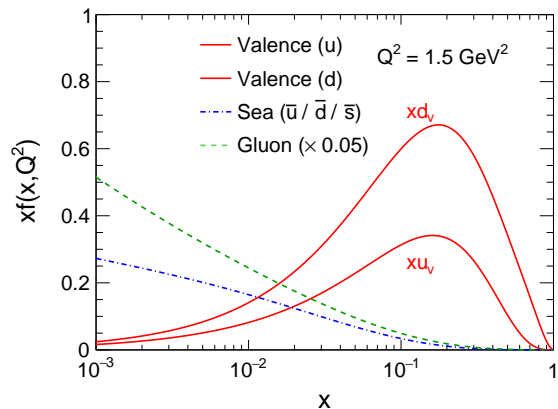


FIG. 2. The predicted valence quark, sea quark and gluon distributions of neutron at  $Q^2 = 1.5 \text{ GeV}^2$  by performing DGLAP evolution equations with the parton-parton recombination corrections to the pure valence quark nonperturbative input from MEM.

quark distribution functions. According to the Quark-Parton model, the structure function [41] is written as,

$$2xF_1(x) = F_2(x) = \sum_i e_i^2 x f_i(x), \quad (10)$$

where the subscript  $i$  is flavor index,  $e_i$  is the electrical charge of the quark flavor  $i$ , and  $x f_i(x)$  is the momentum fraction distribution of the quark of flavor  $i$ . Since valence quarks dominate in the large  $x$  region ( $x > 0.1$ ), the  $F_2(x)$  at large  $x$  mainly comes from the contribution of valence quarks. In the small  $x$  region ( $x < 0.1$ ), the sea quarks begin to make an important contribution to the structure function  $F_2(x)$ .

The BONuS experiment at JLab [5, 7] is via tagging very low momentum spectra protons to measure the  $F_2^n$  of the nearly free neutron from the semi-inclusive scattering of electron off the deuteron. This experimental method minimizes

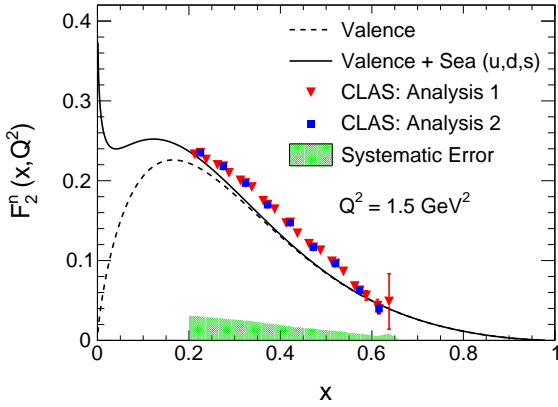


FIG. 3. The predicted structure function of neutron  $F_2^n$  as a function of Bjorken  $x$  compared with the BONuS experiment, where Analysis 1 (triangles) of BONuS experiment performs the Monte Carlo method and the Analysis 2 (squares) performs the ratio method. The solid curve includes the contribution of the sea quarks and the valence quarks, while the dashed curve includes only the valence quark contribution. The systematic uncertainties of the Monte Carlo method in  $F_2^n$  extraction are shown as the green shaded band [7].

the off-shell effect significantly and reduces the nuclear binding uncertainties by picking the spectator protons of momentum below 100 MeV/c and backward angles greater than 100 degrees. These selections ensure that the scattering occurs on the nearly free neutrons. The current  $F_2^n$  data collection cover the nucleon-resonance and deep-inelastic regions with a wide range of Bjorken variable  $x$  under  $0.65 < Q^2 < 4.52$  GeV<sup>2</sup>. Fig. 3 presents our determined  $F_2^n$  as a function of  $x$  compared with BONuS measurements, where the dashed curve only includes the contribution of valence quarks and the solid curve includes the sum of valence quarks and sea quarks. And the Analysis 1 of BONuS experiment is from the Monte Carlo method and the Analysis 2 is from the ratio method. By comparisons, our MEM predictions are consistent with the BONuS data within the systematic uncertainties.

Fig. 4 shows the comparisons between the obtained proton structure function and neutron structure function, from MEM, at  $Q^2 = 12$  GeV<sup>2</sup>. We see that the sea quark distributions only contribute significantly in the small  $x$  region.

### B. Structure Function Ratio $F_2^n/F_2^p$

Figure 5 illustrates the predicted ratio  $F_2^n/F_2^p$  derived from the MEM as a function of the Bjorken variable  $x$ , juxtaposed with previous measurements obtained from deep inelastic scattering (DIS) on deuteron and proton targets. The data from the New Muon Collaboration (NMC), represented by squares, originate from DIS measurements employing a muon beam directed at hydrogen and deuterium [1]. Additionally, the measurements by J. Arrington et al. (circles) provide a systematic analysis of the neutron structure function based

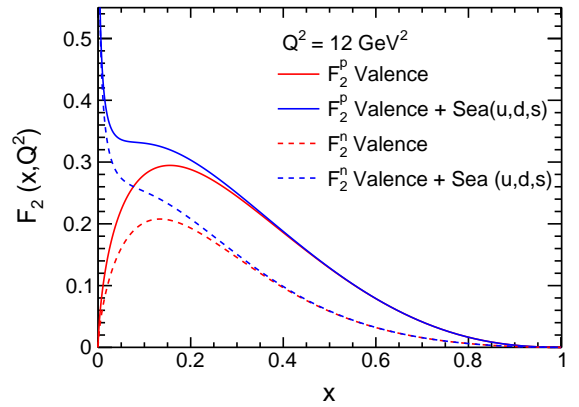


FIG. 4. Comparisons of the structure functions of proton (solid curve) and neutron (dashed curve). The structure function calculations are performed with and without the sea quark distribution.

on deuteron and proton data, incorporating the impulse approximation and an effective two-nucleon mass operator [2]. The triangle markers indicate the  $F_2^n/F_2^p$  ratio extracted after applying deuteron in-medium corrections [3]. In this figure, our predicted structure function ratio  $F_2^n/F_2^p$  from MEM is observed to be slightly lower than the corresponding experimental data, yet remains consistent with global DIS measurements, except for the region where  $x > 0.8$  as reported in Arrington's work. Notably, Arrington's findings reveal a decreasing trend in the  $F_2^n/F_2^p$  ratio as  $x$  increases, a behavior that contrasts with our predictions.

The extraction of free neutron structure information from deuteron data necessitates consideration of various models for nuclear corrections. These include the nuclear density-dependent EMC effect [14, 15], Fermi motion [14], on-shell model extractions [16], and off-shell corrections [17, 18]. A significant challenge posed by these corrections is the inherent fact that deuterons and <sup>3</sup>He, despite their weak binding, do not accurately represent free neutron-proton systems. Furthermore, the employment of differing nuclear correction models can lead to substantial uncertainties in the ratio  $F_2^n/F_2^p$  as  $x$  approaches 1, highlighting the complexities involved in this extraction process.

Fig. 6 shows the predicted ratio  $F_2^n/F_2^p$  at  $Q^2 = 2.2$  GeV<sup>2</sup> compared with the JLab MARATHON experiment [11] and BONuS experiment [7].  $W^*$  here denotes the invariant mass of the final hadrons. The cyan band of the prediction shows the variation of the  $Q^2$ -dependence from 1 GeV<sup>2</sup> to 4.3 GeV<sup>2</sup>. With the quark-hadron duality constrain under the assumption the "scaling" of the elastic form factors as  $q^2 \rightarrow \infty$ , our prediction of the neutron and proton structure function ratio  $F_2^n/F_2^p$  is in excellent agreement with the experimental data. From the Fig. 6, we can see the obvious hadron resonance peaks in BONuS data in the  $0.4 < x < 0.6$  region, even under the invariant mass of the final hadronic state cut of  $W^* > 1.8$  GeV. This is due to the significant non-perturbative quark-gluon interaction and the inclusive lepton-nucleon cross

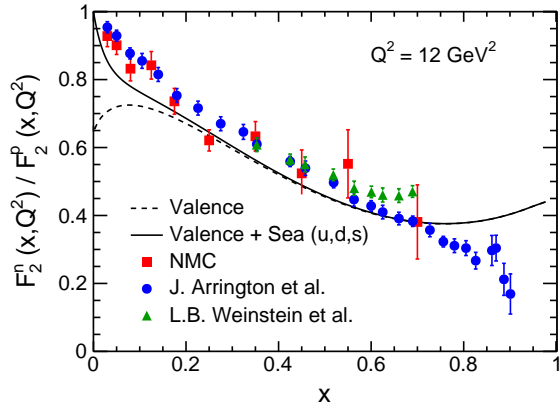


FIG. 5. The obtained structure function ratio of neutron to proton  $F_2^n/F_2^p$  from MEM, compared with the previous experimental extractions. NMC data (squares) are extracted from the simultaneous measurements on hydrogen and deuterium with the incident muon beam [1]. The analysis by J. Arrington et al. (circles) are corrected with the nucleon motion in deuterium [2]. The triangles show  $F_2^n/F_2^p$  data extracted from the deuteron in-medium correction [3]. The errors plotted display the total experimental uncertainties.

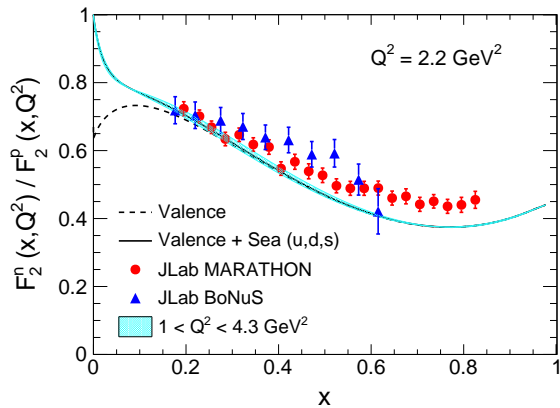


FIG. 6. Comparisons of our predicted  $F_2^n/F_2^p$  ratio with the JLab MARATHON experiment [11] and BONuS experiment [7]. The error bars show the statistical, point to point systematic, and normalization uncertainties of the data. Our theoretical prediction is at  $Q^2 = 2.2 \text{ GeV}^2$ , and the cyan band shows the variation of the scale evolution from  $1 \text{ GeV}^2$  to  $4.3 \text{ GeV}^2$  (in accordance with the experimental data).

section dominated by nucleon resonance at lower energies [8]. However, the JLab MARATHON experiment from measurements of deep inelastic scattering of electrons from  $^3\text{H}$  and  $^3\text{He}$  nuclei eliminates this discrepancy. In Fig. 6, by comparison, we can find that there is a slight difference in magnitude between our prediction results  $F_2^n/F_2^p$  and the JLab MARATHON when  $x > 0.5$ . Our predicted  $F_2^n/F_2^p$  ratio follow the same distribution trend as JLab MARATHON mea-

surements, and the ratio of neutron to proton structure functions stops decreasing with  $x$  increases. In short, the MEM prediction of the ratio  $F_2^n/F_2^p$  successfully describes the measurements of JLab MARATHON and JLab BONuS if the quark-hadron duality assumption is taken into account [8, 35], which also proves the rationality of the quark-hadron duality idea.

### C. $u/d$ ratio of neutron

The  $u/d$  ratio is a quantity which is directly related to the ratio  $F_2^n/F_2^p$ . Fig. 7 shows the predicted  $u/d$  ratio as a function of  $x$  at  $Q^2 = 12 \text{ GeV}^2$ . MEM in this work gives  $u/d = 0$  at the limit of  $x$  approaching one. In experiment, the  $d/u$  ratio of the proton is usually extracted from the  $F_2^n/F_2^p$  data, neglecting the strange quark contribution. Note that the  $d/u$  ratio of the proton equals the  $u/d$  ratio of the neutron under the assumption of isospin symmetry.

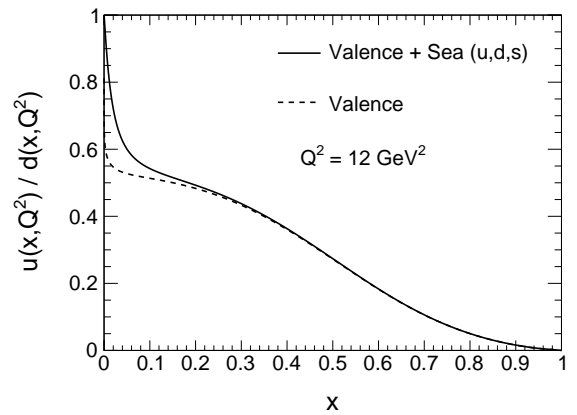


FIG. 7. The  $u/d$  ratio of the neutron at  $Q^2 = 12 \text{ GeV}^2$  given by MEM. The solid curve includes also the sea quark contributions, while the dashed curve is calculated from the valence quark distributions only.

Table I lists the comparisons of our predicted  $F_2^n/F_2^p$  ratio and  $u/d$  ratio of neutron at the limit of  $x \rightarrow 1$ , compared with other theoretical predictions. The structure function ratio between neutron and proton is denoted as  $R^{n/p}(x) = F_2^n(x)/F_2^p(x)$  in this work for the convenience of discussions. In this work by MEM, we find that  $R^{n/p}(0) \approx 1.0$  to  $R^{n/p}(1) \approx 0.47$ , which is clearly depicted in Fig. 5.  $R^{n/p}(0) \approx 1.0$  is due to the fact that the sea quark distribution dominates at small  $x$ . The other result is that  $u^n/d^n \approx 0$  when  $x$  approaches one. Our result is quite different from the predictions from the exact spin-flavor SU(6) symmetry, the perturbative QCD assuming the helicity conserved quarks interacted via hard gluon exchange [42], and the quark counting rule method [43]. However the models with the SU(6) symmetry breaking via the scalar diquark dominance [44, 45] predict the very similar result of ours. In addition, the hyperfine-perturbed quark model also makes a

TABLE I. The list of the theoretical predictions of  $R^{n/p} = F_2^n/F_2^p$  and  $u^n/d^n$  at the limit of  $x \rightarrow 1$  from different models.

	$R^{n/p}$	$u^n/d^n$
SU(6) Flavor Symmetry	2/3	1/2
Perturbative QCD	3/7	1/5
Quark Counting Rule	3/7	1/5
Diquark (Feynman)	1/4	0
Quark Model (Isgur)	1/4	0
MEM (this work)	0.47	0

prediction that similar to ours [46]. These predictions at large  $x$  are needed to be tested in the future experiments.

#### D. Assessment of Isospin Symmetry

To investigate the degree of isospin symmetry between the proton and neutron, we have examined the differences in their valence quark distributions and first-order moments. These comparisons are presented in Fig. 8, where panel (a) and panel (b) display the differences in valence quark distributions and first-order moments, respectively. By analyzing the results, it is evident that at intermediate values of  $x$  ( $0.02 < x < 0.5$ ), the isospin symmetry between the proton and neutron is indeed violated, whereas at the limits  $x \sim 0$  and  $x = 1$ , the symmetry appears to be preserved.

Furthermore, inspection of the first-order moments shown in panel (b) reveals a maximal difference of 0.0017 between the two nucleons at low  $Q^2$ , and a gradual recovery of the isospin symmetry as  $Q^2$  increases. While the results in Fig. 8 clearly demonstrate the presence of isospin breaking, the magnitude of this effect is found to be moderate.

The minor isospin symmetry breaking between the proton and neutron could be attributed to differences in their initial valence quark distributions, as well as variations in their charge radii and masses. These differences in nucleon properties may contribute to the observed isospin breaking and warrant further investigation to clarify their role in the quark structure of the nucleon.

#### IV. SUMMARY

The maximum entropy method offers a novel and efficient approach for predicting the nonperturbative structure of nucleons, particularly for neutron, where experimental data are scarce. By imposing constraints from quark models, quark-hadron duality, and quark confinement, MEM can be used to determine a reasonable initial valence quark distribution for the neutron. Our analysis reveals that at an initial scale  $Q_0^2$ , the neutron is composed of three valence quarks with no sea quark or gluon distributions. The predicted ratio of the valence structure functions between neutron and proton,  $F_2^n/F_2^p$ , is found to be consistent with current JLab experimental data

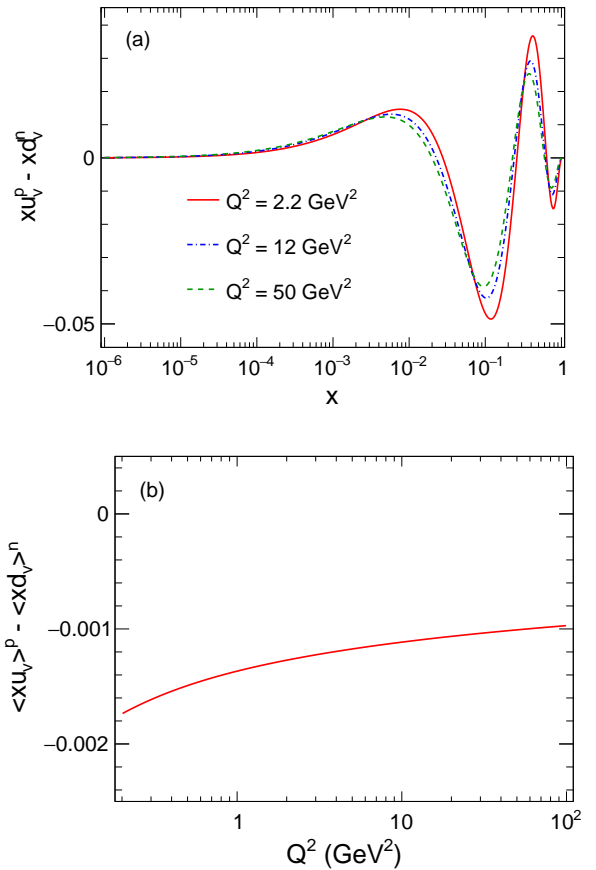


FIG. 8. Panel (a) The valence quark distribution difference between proton and neutron as a function of Bjorken variable  $x$ . Panel (b) The difference of the first-order moments of valence quark distributions between proton and neutron as a function of  $Q^2$ .

and world deep inelastic scattering (DIS) data. The nearly free neutron measurements by the JLab MARATHON and BONuS collaborations provide a crucial test of our predictions from MEM. By considering the contamination from nucleon resonances, our results show that the obtained  $F_2^n/F_2^p$  ratio is in agreement with JLab BONuS experimental results, while the higher energy MARATHON measurements remove the contamination and provide a clear test of our predictions. Furthermore, our analysis reveals that the large- $x$  behaviors of  $F_2^n/F_2^p$  and  $u^n/d^n$  are consistent with perturbative QCD and quark counting rule predictions, but deviate from SU(6) flavor symmetry, diquark model, and quark model predictions. Finally, our results show that the isospin breaking between proton and neutron is minor, and may arise from differences in initial valence quark input, charge radius, and mass between proton and neutron.

## ACKNOWLEDGMENTS

This work is supported by the National Natural Science Foundation of China under the Grant NO. 12305127, the

International Partnership Program of the Chinese Academy of Sciences under the Grant NO. 016GJHZ2022054FN. and National Key R&D Program of China under the Grant NO. 2024YFE0109802.

- 
- [1] P. Amaudruz *et al.* (New Muon), Nucl. Phys. B **371**, 3 (1992).  
[2] J. Arrington, F. Coester, R. J. Holt, and T. S. H. Lee, J. Phys. G **36**, 025005 (2009), arXiv:0805.3116 [nucl-th].  
[3] L. B. Weinstein, E. Piasetzky, D. W. Higinbotham, J. Gomez, O. Hen, and R. Shneur, Phys. Rev. Lett. **106**, 052301 (2011), arXiv:1009.5666 [hep-ph].  
[4] J. Arrington, J. G. Rubin, and W. Melnitchouk, Phys. Rev. Lett. **108**, 252001 (2012), arXiv:1110.3362 [hep-ph].  
[5] N. Baillie *et al.* (CLAS), Phys. Rev. Lett. **108**, 142001 (2012), [Erratum: Phys.Rev.Lett. 108, 199902 (2012)], arXiv:1110.2770 [nucl-ex].  
[6] O. Hen, E. Piasetzky, R. Shneur, L. B. Weinstein, and D. W. Higinbotham, (2011), arXiv:1109.6197 [hep-ph].  
[7] S. Tkachenko *et al.* (CLAS), Phys. Rev. C **89**, 045206 (2014), [Addendum: Phys.Rev.C 90, 059901 (2014)], arXiv:1402.2477 [nucl-ex].  
[8] I. Niculescu *et al.*, Phys. Rev. C **91**, 055206 (2015), arXiv:1501.02203 [hep-ex].  
[9] A. Accardi, L. T. Brady, W. Melnitchouk, J. F. Owens, and N. Sato, Phys. Rev. D **93**, 114017 (2016), arXiv:1602.03154 [hep-ph].  
[10] H. Szumila-Vance, C. Keppel, S. Escalante, and N. Kalantarians, Phys. Rev. C **103**, 015201 (2021), arXiv:2002.02597 [nucl-ex].  
[11] D. Abrams *et al.* (Jefferson Lab Hall A Tritium), Phys. Rev. Lett. **128**, 132003 (2022), arXiv:2104.05850 [hep-ex].  
[12] H. C. Fenker *et al.*, Nucl. Instrum. Meth. A **592**, 273 (2008).  
[13] S. Li, A. Accardi, M. Cerutti, I. P. Fernando, C. E. Keppel, W. Melnitchouk, P. Monaghan, G. Niculescu, M. I. Niculescu, and J. F. Owens, Phys. Rev. D **109**, 074036 (2024), arXiv:2309.16851 [hep-ph].  
[14] L. W. Whitlow, E. M. Riordan, S. Dasu, S. Rock, and A. Bodek, Phys. Lett. B **282**, 475 (1992).  
[15] L. L. Frankfurt and M. I. Strikman, Phys. Rept. **160**, 235 (1988).  
[16] J. Gomez *et al.*, Phys. Rev. D **49**, 4348 (1994).  
[17] W. Melnitchouk, A. W. Schreiber, and A. W. Thomas, Phys. Lett. B **335**, 11 (1994), arXiv:nucl-th/9407007.  
[18] W. Melnitchouk and A. W. Thomas, Phys. Lett. B **377**, 11 (1996), arXiv:nucl-th/9602038.  
[19] K. Nakano and S. S. M. Wong, Nucl. Phys. A **530**, 555 (1991).  
[20] R. J. Holt and C. D. Roberts, Rev. Mod. Phys. **82**, 2991 (2010), arXiv:1002.4666 [nucl-th].  
[21] R. Wang and X. Chen, Phys. Rev. D **91**, 054026 (2015), arXiv:1410.3598 [hep-ph].  
[22] C. Han and X. Chen, Chin. Phys. C **41**, 113103 (2017), arXiv:1612.06631 [hep-ph].  
[23] C. Han, H. Xing, X. Wang, Q. Fu, R. Wang, and X. Chen, Phys. Lett. B **800**, 135066 (2020), arXiv:1809.01549 [hep-ph].  
[24] C. Han, G. Xie, R. Wang, and X. Chen, Eur. Phys. J. C **81**, 302 (2021), arXiv:2010.14284 [hep-ph].  
[25] C. Han, W. Kou, X. Wang, and X. Chen, Eur. Phys. J. C **84**, 1067 (2024), arXiv:2407.05923 [hep-ph].  
[26] X. Chen, J. Ruan, R. Wang, P. Zhang, and W. Zhu, Int. J. Mod. Phys. E **23**, 1450057 (2014), arXiv:1306.1872 [hep-ph].  
[27] R. Wang, X. Chen, and Q. Fu, Nucl. Phys. B **920**, 1 (2017), arXiv:1611.03670 [hep-ph].  
[28] R. Wang and X. Chen, Chin. Phys. C **41**, 053103 (2017), arXiv:1609.01831 [hep-ph].  
[29] X. Chen, J. Ruan, R. Wang, P. Zhang, and W. Zhu, Eur. Phys. J. Plus **131**, 6 (2016), arXiv:1404.0759 [hep-ph].  
[30] G. Parisi and R. Petronzio, Phys. Lett. B **62**, 331 (1976).  
[31] A. I. Vainshtein, V. I. Zakharov, V. A. Novikov, and M. A. Shifman, JETP Lett. **24**, 341 (1976).  
[32] M. Gluck and E. Reya, Nucl. Phys. B **130**, 76 (1977).  
[33] M. Glück, E. Reya, and A. Vogt, Eur. Phys. J. C **5**, 461 (1998), arXiv:hep-ph/9806404.  
[34] J. Pumplin, D. R. Stump, J. Huston, H. L. Lai, P. M. Nadolsky, and W. K. Tung, JHEP **07**, 012 (2002), arXiv:hep-ph/0201195.  
[35] E. D. Bloom and F. J. Gilman, Phys. Rev. D **4**, 2901 (1971).  
[36] K. G. Wilson, Phys. Rev. D **10**, 2445 (1974).  
[37] P. Zyla *et al.*, Prog. Theor. Exp. Phys **2020**, 083C01 (2020).  
[38] Y. L. Dokshitzer, Sov. Phys. JETP **46**, 641 (1977).  
[39] V. N. Gribov and L. N. Lipatov, Sov. J. Nucl. Phys. **15**, 438 (1972).  
[40] G. Altarelli and G. Parisi, Nucl. Phys. B **126**, 298 (1977).  
[41] C. G. Callan, Jr. and D. J. Gross, Phys. Rev. Lett. **22**, 156 (1969).  
[42] G. R. Farrar and D. R. Jackson, Phys. Rev. Lett. **35**, 1416 (1975).  
[43] S. J. Brodsky, M. Burkardt, and I. Schmidt, Nucl. Phys. B **441**, 197 (1995), arXiv:hep-ph/9401328.  
[44] R. P. Feynman, *Photon-hadron interactions* (CRC Press, 2018).  
[45] F. E. Close, Phys. Lett. B **43**, 422 (1973).  
[46] N. Isgur, Phys. Rev. D **59**, 034013 (1999), arXiv:hep-ph/9809255.